Field-Aligned Electron Density Distribution of the Inner Magnetosphere Inferred from Coordinated Observations of Arase and Van Allen Probes

Yuki Obana[1], Yukinaga Miyashita[2], Naomi Maruyama[3], Atsuki Shinbori[4], Masahito Nosé[5], Masafumi Shoji[5], Atsushi Kumamoto[6], Fuminori Tsuchiya[6], Shoya Matsuda[7], Ayako Matsuoka[8], Yoshiya Kasahara[9], Yoshizumi Miyoshi[4], Iku Shinohara[7], William S Kurth[10], Charles W. Smith[11], and Robert John MacDowall[12]

[1]Osaka Electro-Communication University
[2]Korea Astronomy and Space Science Institute
[3]University of Colorado
[4]Institute for Space-Earth Environmental Research, Nagoya University
[5]Nagoya University
[6]Tohoku University
[7]Japan Aerospace Exploration Agency
[8]Kyoto University
[9]Kanazawa University
[10]University of Iowa
[11]University of New Hampshire
[12]NASA Goddard Space Flight Center

November 22, 2022

Abstract

The RBSP and the Arase satellites have different inclinations and sometimes they fly both near the equator and off the equator on the same magnetic field line, simultaneously. Such conjunction events give us opportunities to compare the electron density at different latitudes. In this study, we analyzed the plasma waves observed by Arase and RBSP-A or B during the three conjunction events during and after the 7 Sep 2017 storm event. The electron number density at the satellite positions were estimated from frequencies of the UHR emissions obtained by the HFA/PWE onboard the Arase and the Waves instrument onboard RBSP, respectively. During the three conjunction events, the satellites passed through the plume, inner trough (the narrow region with low electron density between main body of the plasmasphere and the plume), plasmatrough with variable electron density, and partially-refilled plasmasphere. The power-law index m for the inner trough and plume was inferred to be 6~8 and ~0, respectively. This is interpreted to mean that the trough was close to collisionless and the plume was near diffusive equilibrium. In the plasmatrough with the varying density, both the high-density and low-density regions had m~0. The low-density portion of this region may have a different origin from the inner trough, because of the different m-indices. For the partially-refilled plasmasphere in the storm recovery phase, the power-law index m showed negative values, meaning that the density in the equatorial plane was higher than at higher latitudes.

1

1   Field-Aligned Electron Density Distribution of the Inner Magnetosphere Inferred from
2   Coordinated Observations of Arase and Van Allen Probes
3

4   Yuki Obana[1]*, Yukinaga Miyashita[2], Naomi Maruyama[3,4], Atsuki Shinbori[5], Masahito Nosé[5],
5   Masafumi Shoji[5], Atsushi Kumamoto[6], Fuminori Tsuchiya[7], Shoya Matsuda[8], Ayako
6   Matsuoka[9], Yoshiya Kasahara[10], Yoshizumi Miyoshi[5], Iku Shinohara[8], William S. Kurth[11],
7   Charles W. Smith[12], Robert J. MacDowall[13]

8

9   [1]Department   of   Engineering   Science,   Faculty   of   Engineering,   Osaka
10 Electro-Communication University, 18-8 Hatsucho, Neyagawa, Osaka, 572-8530, Japan.
11 [2]Korea Astronomy and Space Science Institute, Daejeon, South Korea.
12 [3]CIRES, University of Colorado Boulder, CO, 80305, USA.
13 [4]NOAA Space Weather Prediction Center, CO, 80305, USA.
14 [5]Institute for Space-Earth Environmental Research (ISEE), Nagoya University, Nagoya,
15   Aichi, 464-8601, Japan.
16 [6]Department of Geophysics, Tohoku University, Aoba-ku, Sendai, Miyagi, 980-8578,
17   Japan.
18 [7]Planetary Plasma and Atmospheric Research Center (PPARC), Tohoku University, Aoba-ku,
19   Sendai, Miyagi, 980-8578, Japan.
20 [8]Institute of Space and Astronautical Science, Japan Aerospace Exploration Agency,
21   3-1-1, Yoshinodai, Chuo-ku, Sagamihara, Kanagawa, 252-5210, Japan.
22 [9]Data Analysis Center for Geomagnetism and Space Magnetism Graduate School of Science,
23   Kyoto University, Kyoto, 606-8502, Japan.
24 [10] Graduate School of Natural Science and Technology, Kanazawa University,
25   Kakumamachi, Kanazawa, 920-1192, Japan.
26 [11] Department of Physics and Astronomy, University of Iowa, Iowa City, IA, USA
27 [12] nstitute for the Study of Earth, Oceans, and Space, University of New Hampshire,
28   Durham, NH, USA
29 [13] Solar System Exploration Division, Goddard Space Flight Center, Greenbelt, MD, USA
30
31 *Corresponding author: Yuki Obana (obana@osakac.ac.jp)
32

33 **Key Points:**

34   Using in-situ measurements of the electron density from Arase and RBSP, we

35   estimated the density distribution along magnetic field lines.

36   The power-law index of the electron density distributions was 6~8, ~0 and -2~-1

37   for the trough, plume and partially refilled plasmasphere, respectively.

38   This is the first estimation of the power-law index using the data from

39   different spacecraft projects.

40

41 **Plain Language Summary**

42   The plasmasphere is the region filled with cold, dense ionized gas in geospace.
43 The ionized gas mainly consists protons, helium ions, oxygen ions and electrons, which
44 come from Earth's ionosphere and fill magnetic flux tubes. The density distribution
45 of the ionized gas along the flux tube provides important information to understand
46 how the ions and electrons have been supplied from the ionosphere. Many satellites
47 fly in the equatorial plane, hence, do not provide information on the electron density
48 along the field. The RBSP and the Arase satellites have different inclinations and
49 sometimes they simultaneously fly near the equator and off the equator on the same
50 magnetic field line. Using electron densities observed by these satellites during
51 the 7 Sep 2017 storm, we successfully estimated the electron density distribution
52 along of the field lines inside the partially refilled plasmasphere, outside of the
53 plasmasphere and in the tail-like structure called a plume.
54

55 **Abstract**

56   The RBSP and the Arase satellites have different inclinations and sometimes they
57 fly both near the equator and off the equator on the same magnetic field line,
58 simultaneously. Such conjunction events give us opportunities to compare the electron
59 density at different latitudes. In this study, we analyzed the plasma waves observed
60 by Arase and RBSP-A or B during the three conjunction events during and after the
61 7 Sep 2017 storm event. The electron number density at the satellite positions were
62 estimated from frequencies of the UHR emissions obtained by the HFA/PWE onboard the
63 Arase and the Waves instrument onboard RBSP, respectively. During the three
64 conjunction events, the satellites passed through the plume, inner trough (the narrow
65 region with low electron density between main body of the plasmasphere and the plume),
66 plasmatrough with variable electron density, and partially-refilled plasmasphere.
67 The power-law index m for the inner trough and plume was inferred to be 6~8 and ~0,
68 respectively. This is interpreted to mean that the trough was close to collisionless

69 and the plume was near diffusive equilibrium. In the plasmatrough with the varying
70 density, both the high-density and low-density regions had $\tilde{m} 0$. The low-density
71 portion of this region may have a different origin from the inner trough, because
72 of the different m-indices. For the partially-refilled plasmasphere in the storm
73 recovery phase, the power-law index m showed negative values, meaning that the density
74 in the equatorial plane was higher than at higher latitudes.
75
76 ## 1. Introduction
77   The plasmasphere is a region in the inner magnetosphere filled with cold, dense
78 plasma from the underlying ionosphere, and the field-aligned profile of its density
79 attracts much interest, because it reflects the physical processes of mass transport
80 from the source region. For example, when the very simple power law model

$$n = n_{eq} \left(\frac{LR_E}{R} \right)^m$$

81 is used, where n_{eq} is the density on the equatorial plane, L is the magnetic L-shell
82 parameter, R_E is Earth radius, R is geocentric distance to the observation point and
83 m is the power-law index. The density profile for diffusive equilibrium is closed,
84 having a low-m (m=0.5~1) power law distribution, whereas, the density profile for
85 collisionless plasma corresponds to high-m ($\tilde{m} 4$) power law distributions (Eviatar
86 et al., 1964; Angerami and Carpenter, 1966; Takahashi et al., 2004).
87   We have, however, few opportunities to investigate the field aligned profile
88 of plasma density from actual observational data. Previous studies have been done
89 using (i) in-situ measurements of electron density from plasma wave data by polar
90 orbiting spacecraft (e.g., Goldstein et al., 2001; Denton et al., 2002; Sandhu et
91 al., 2016), (ii) passive remote sensing of electron density with whistler waves (e.g.,
92 Angerami and Carpenter, 1966), (iii) passive remote sensing of plasma mass density
93 with harmonic frequencies of standing Alfven waves in the ultra-low frequency (ULF)
94 range (e.g., Takahashi et al., 2004; Denton et al., 2009), (iv) active remote sensing
95 of electron density by the radio plasma imager (RPI) onboard the Imager for
96 Magnetopause-to-Aurora Global Exploration (IMAGE) satellite (Reinisch et al., 2001;
97 Huang et al., 2004).
98   Goldstein et al. (2001) used the electron density measurements of the Polar
99 satellite and obtained a power-law index of $m = 0.37 \pm 0.8$ for high density regions
100 (n_e>100/cc) and 1.7 $\pm$ 1.1 for low density regions (n_e<100/cc). Denton et al. (2002)
101 used same data set as Goldstein et al. (2001) and estimated a power-law index of 1.6-
102 2.1 for the plasmatrough. Takahashi et al. (2004) estimated the power-law index of

the plasma mass density and found that $m \sim 0.5$ at $4<L<6$, which is consistent with a diffusive equilibrium solution. On the other hand, no single value of m fit the average observed frequency ratios at $6<L<7$, and the theoretical solutions indicated that the mass density was peaked at the equator. The subsequent studies by Denton et al. (2009) and Sandhu et al. (2016) analyzed Cluster data and showed that the electron density also had a local maximum in density near the equator in the plasmatrough. As described above, many results have been obtained in which both electrons and ions have had a density distribution close to diffusion equilibrium as long as they have been in the high-density region in the plasmasphere. Also, in high L-shell regions with low density, power-law indices m have had larger values or have not tended to take a specific value, which implied that there may have been a local maximum in density near the equatorial plane.

In recent years, the exploration of the inner magnetosphere has entered the multi-point observation era with satellites flying in formation. In order to obtain a comprehensive understanding of the acceleration, transport, and loss of relativistic electrons in the radiation belts, cross-energy coupling of the inner magnetospheric plasma has been of prime interest. (Miyoshi et al., 2016; 2018a). To understand the detailed cross-energy coupling processes, it is necessary to know all parameters that contribute to the coupling. Despite the fact that the plasmasphere is the lowest energy population in the inner magnetosphere, it is also important, because it dominates the background plasma environment which controls wave dispersion and resonance conditions. Moreover, the latitudinal distribution of plasma density significantly controls propagations of plasma waves.

In this paper, we show simultaneous measurements of the plasma density along the same magnetic field by proposing a new method for examining the density profile along the magnetic field lines of plasma electron density at Arase (Exploration of energization and Radiation in Geospace: ERG) satellite (Miyoshi et al., 2018a) and Van Allen probes (the Radiation Belt Storm Probes: RBSP, Mauk et al., 2013) era. We estimate the power-law index of three events during and after the 7 September 2017 storm event using in-situ measurements of the electron number density from Arase and RBSP whose orbits have different inclinations. This gives instantaneous information about the density profile along field lines. Thus, it provides an opportunity to capture dynamic changes of the plasmasphere during magnetic storms.

2. Simultaneous Observations by Arase and RBSP-B
2.1. Satellite orbits

139   Figure 1 shows the positions of Arase (the red line with circles) and RBSP-B (the
140   blue line with triangles) in the L-value-Magnetic Local Time (MLT) plane (top) and
141   L-value-Magnetic Latitude plane (bottom) during the conjugate event on 8 Sep 2017
142   when the spacecraft pass the same L-value (L = 3.3-4.1). The exact time of the two
143   orbits are indicated in the top panel. The small circles and triangles on the orbits
144   respectively indicate every five-mins positions of Arase and RBSP-B. The L-value,
145   MLT and magnetic latitude of the satellites were calculated by using
146   Olson-Pfitzer-Quitet (OPQ 77) magnetic field model (Olson and Pfitzer, 1977), and
147   the L-value is McIlwain L-parameter (McIlwain, 1961) for particles with a pitch angle
148   of 90 degrees. Their orbits seem to cross in the afternoon sector. In fact, the
149   difference of MLT and UT comparing at the same L-values are less than 0.5 hr and 15
150   mins, respectively. Such a conjunction event provides a good opportunity to compare
151   the electron density between the two different latitudes due to the difference of
152   inclinations of Arase and RBSP. As shown in the bottom panel of Figure 1, Arase was
153   ~10 degrees higher in latitude than RBSP-B.
154
155   **2.2. Evolution of the Plasmasphere during the 7 Sep 2017 Storm Event**
156   The top and middle panels of Figure 2 respectively display temporal variations
157   of the Kp and SYM-H indices during the interval of 6-10 Sep 2017. They indicate that
158   a magnetic storm with two main phases commenced around 0 UT on 8 Sep and disturbances
159   continued for approximately 30 hrs, followed by a gradual recovery phase. This storm
160   has been considered to be a CME (coronal mass ejection)-driven storm. The blue, green,
161   black and magenta bars in the middle panel indicate the time intervals when the
162   electron density, shown in the bottom panel of this figure were observed. The event
163   numbers in parentheses are the event numbers defined in Sections 2-3, 2-4 and 2-5.
164   A detailed description of the plasmaspheric dynamics during this storm event is
165   given by Obana et al. (2019), therefore, here we give only a brief description. The
166   bottom panel of Figure 2 shows L-value distribution of electron density obtained by
167   the Arase observations. The exact times are given in the panel. The blue line (0)
168   indicates a plasmasphere which spreads to L ~5 before the storm. The green line (1)
169   shows that the plasmasphere has eroded to L=2.5 during the second main phase. In L
170   >3 of the green line profile, the density shows jagged structures. It implies that
171   the satellite was in the plasmatrough with variations in electron density. In black
172   (2), the plasmasphere has been extremely eroded and the plasmapause reached around
173   L = 1.6-1.7. An isolated increase in density appears to be a plume at L = 3.4-4.3.
174   The magenta line (3) was obtained two days after the magnetic storm entered the second

175 recovery phase, and the eroded plasmasphere has partially refilled.

176

2.3. Event #1: 23:20 UT on 8 Sep 2017

178 Figure 3 shows the plasma wave observations from Arase and RBSP-B and locations
179 of the satellites during 23:20 UT on 8 Sep - 00:10 UT on 9 Sep 2017. Figure 3a is
180 the plasma wave spectrogram for the electric field in the frequency range of 10-400
181 kHz measured by the onboard frequency analyzer (OFA) and the high-frequency analyzer
182 (HFA) of the Plasma Wave Experiment (PWE) (Kasahara et al., 2018; Kumamoto et al.,
183 2018). The clear emissions of the Upper Hybrid Resonance (UHR) waves is identified
184 by the white line and arrow. The UHR frequency was decreasing gradually from 300 to
185 100 kHz during 23:20-23:48 UT because Arase was in an outbound pass, and then suddenly
186 jumped up to ~150 kHz at 23:49 UT. This implies that the satellite passed the boundary
187 between the low- and high-density regions, which correspond to the inner trough and
188 plasma plume, respectively.

189 Figure 3b shows the plasma wave spectrogram for electric fields for RBSP-B. These
190 data were measured by the Electric and Magnetic Field Instrument Suite and Integrated
191 Science (EMFISIS) Wave instrument (Kletzing et al., 2013). The UHR waves can be seen
192 as indicated by the white line and arrow and its frequency gradually increased since
193 RBSP-B was in an inbound pass. Its frequency raised in stepwise fashion at 23:21 UT
194 and decreased around 23:50 UT. This implies that the satellite passed the plume and
195 came into the inner trough around 23:50 UT.

196 Figure 3c-e respectively show the L-value, MLT and magnetic latitude of Arase
197 (the red line) and RBSP-B (the blue line). They are calculated using the OPQ77 magnetic
198 field model, because this time interval is in the recovery phase of the storm. The
199 thick parts of the lines indicate each value as the satellites passed L=3.3-4.1. In
200 this L-value range, the two satellites passed the points with same L-values with time
201 differences of less than 30 mins. The differences in MLT between Arase and RBSP-B
202 were less than 0.5 hr. Due to the difference of inclinations, the magnetic latitudes
203 of Arase were ~10 degrees higher than that of RBSP-B.

204 From the upper-limit frequency of the UHR waves (f_{UHR}), the electron density n_e along
205 the spacecraft orbit is estimated using the following equation

$$n_e = \frac{f_{UHR}^2 - f_{ce}^2}{8980^2},$$

206 where f_{ce} is the electron cyclotron frequency. The densities and frequencies are
207 expressed in cubic centimeters and in hertz, respectively. In this paper, the local
208 f_{ce} was calculated from the spin average total magnetic field intensity measured by

209　the Magnetic Field Experiment (MGF) instrument (Matsuoka et al., 2018) onboard Arase
210　or the EMFISIS magnetometer onboard RBSP.

211　　The upper panel of Figure 4 shows the electron number density profiles as a function
212　of L. A density jump can be seen around L~3.45 in the Arase observations (red) and
213　around L~3.57 in the RBSP-B observations (blue), respectively. These jumps correspond
214　to the boundary between the inner trough and plume. The difference in the L-values
215　of the boundaries between Arase and RBSP-B may be due to the difference of MLT of
216　the satellites.

217　　Interestingly, the two satellites differed in magnetic latitude by as much as 10
218　degrees, but in the plume, n_e shows similar values at same L-values. That is, the
219　density of the plume seems to be almost uniform at least in the magnetic latitude
220　range of 10-30°. Whereas in the inner trough, the n_e at higher latitudes (Arase) is
221　higher. That is, the n_e changes rather steeply along the field line.

222　　Assuming a power-law density distribution as function of geocentric distance, the
223　power-law index m can be calculated as

$$m = -\frac{\ln(n_{e1}/n_{e2})}{\ln(R_1/R_2)}$$

224　and shown in the lower panel of Figure 4. Where the subscripts "1" and "2" indicate
225　values for satellites #1 and #2. For this calculation, moving averages of n_e with a
226　0.05 of window width in L-value were used. The m index is plotted in the panel only
227　if both relative standard deviations (the ratio of the standard deviation to the
228　average) of n_e of Arase and RBSP-B in the window are less than 25 %. The m indices
229　were 4 to 7 and -3 to 0 in the inner trough and plume, respectively. These are indicated
230　in the lower panel of Figure 4.

231

232　**2.4.　Event #2: 14:15 UT on 8 Sep 2017**

233　　Figure 5 shows the plasma wave observations and locations of Arase and RBSP-B
234　during the interval 14:15-15:05 UT on 8 Sep 2017, in the same format as Figure 3,
235　but L-value, MLT and magnetic latitude are calculated using the Tsyganenko 2004 storm
236　time model (T04s, Tsyganenko and Sitnov, 2005), because this period is in the second
237　main phase of the storm. The clear emissions of the UHR waves are found as shown by
238　the white lines and arrows. The UHR frequency fluctuates with the time scale of the
239　range from 1 to 10 min. The timing of the fluctuations seems to be inconsistent between
240　the two satellites, thus, it is surmised that this change in frequency does not reflect
241　the time change of the electron density, but reflects the spatial variation. As shown
242　in Figure 2, this observation is during the second main phase, with a plasmapause

243 seen at L=2.5, thus, the fluctuations of f_{UHR} shown in Figure 5 implies existence of
244 small-scale structures in the plasmatrough.

245 Results showing this expectation are given in Figure 6. The upper panel of Figure
246 6 shows the electron number density profiles as a function of the McIlwain's
247 L-parameter calculated using the T04s model during Event #2. At least between L =
248 3.3 and 3.9, the changes in electron density observed by Arase and RBSP-B seem to
249 be correlated.

250 Using ~10 degrees as the difference in magnetic latitudes (Figure 5e), the m index
251 was calculated as shown in the bottom panel of Figure 6. In both the high- and low-
252 density regions, the derived m index has small values (typically ~0). Obviously, the
253 very large negative values for L>3.9 are meaningless, because the fluctuations in
254 electron densities observed by Arase and RBSP-B are not correlated each other in this
255 region.

256

257 ## 2.5.   Event #3: 13:40 UT on 10 Sep 2017

258 The third event is a conjunction of Arase and RBSP-A, during the interval of 13:40-
259 14:30 UT on 10 Sep, in the recovery phase of the storm. Figure 7 (same format as Figure
260 3) shows a simple picture of emission. The f_{UHR} observed by Arase gradually decreased
261 from 200 to 70 kHz, and those observed by RBSP-A gradually increased from 100 to 200
262 kHz. This corresponds to the gradual electron density gradient with distance. The
263 time of this event is about two days after the commencement of the second recovery
264 phase, thus the observations depict the density profiles of a partially refilled
265 plasmasphere (Figure 2).

266 Figure 8 shows the n_e obtained by Arase and RBSP-A observations (upper) and the
267 inferred m index (bottom) in the same format as Figure 4. Interestingly, the electron
268 density observed by RBSP-A was higher than that by Arase, despite RBSP-A being at
269 a lower latitude. Because plasmaspheric plasma is supplied from the underlying
270 ionosphere, the density is usually lower in near the equator. However, our results
271 suggest a profile opposite to this. The bottom panel of Figure 8 shows m index, which
272 has negative values due to the higher electron density near the equator.

273

274 ## 3. Discussion.

275 ### 3.1. Accuracy and coverage of this study

276 The three conjunction events shown in this study have <45 mins difference in UT
277 and <1 hr difference in MLT when the two satellites cross flux tubes with same L-value.
278 The L-value includes an uncertainty of 0.05 derived from the window width used for

279   the moving average of n_e.

280   Comparing to previous studies, IMAGE-RPI sounding takes only two minutes to make

281   one survey (Song et al., 2005). On the other hand, studies using polar orbiting

282   satellites, take several hours until the satellite passes two points of the flux tube

283   with the same L-value (Goldstein et al.,2001). Our surveys have time accuracies

284   intermediate to those studies.

285   Next, we compare our time accuracies with the time scale of dynamic changes of

286   the plasmasphere. According to Obana et al. (2010), the refilling rates at L = 3.8

287   were estimated to be 13 amu/cm^3/hr, so assuming that all the ions are protons, the

288   electron density will increase 10/cm^3 in 45 mins. Even in low-density regions (n_e~100

289   /cm^3), this is only a 10% increase in density. On the other hand, Goldstein et al.

290   (2003) investigated images of the He$^+$ plasmasphere taken by the IMAGE-EUV camera and

291   reported that the nightside plasmapause had moved inward by ~2 R_E in 3 hrs during the

292   erosion. In such a case, density changes more quickly, and thus, more precise

293   conjunctions (with shorter time differences) will be required.

294   The difference in MLT must be considered when structures that change in both radial

295   and azimuthal directions, like the plume, are considered. In fact, as shown in Figure

296   4, the position of the inner edge of the plume observed by Arase and RBSP were displaced

297   by 0.12 R_E. This may be due to the difference in MLT.

298   The coverage of magnetic latitudes should also be considered. The satellites used

299   in this study explore magnetic latitudes of < 30 degrees (Arase) and <10 degrees (RBSP).

300   Note that the m indices presented in this study do not represent the entire magnetic

301   field line, but only in this range.

302

303   ## 3.2. Power-law index for the inner trough and the plume

304   In Event #1, the power-law index shows respectively m >4 at L=3.3-3.4 (inner

305   trough), and m ~0 at L=3.6-4.1 (plume). This is interpreted as the inner trough being

306   close to collisionless and the plume being near diffusive equilibrium. Previous

307   studies explained that the plume and inner trough are formed by the convection electric

308   field which cause sunward motion of the plasma, the subsequent corotation and the

309   subauroral polarization stream (SAPS) electric field. Based on this idea, the plumes

310   originate in the main body of the plasmasphere and inner troughs originate in the

311   low-density region (so-called outer trough) after the plasmasphere shrank. Our

312   results do not conflict with this model.

313

314   ## 3.3. Negative power law index in the partial refilling region

315   In Event #3, power-law index m shows negative values, meaning that the density
316   in the equatorial plane is higher than off the equator. The plasmaspheric density
317   is generally higher closer to Earth. This reflects that the plasma is of ionospheric
318   origin. However, the electron density in Event #3 shows the opposite features. How
319   can these results be explained?

320   The period of Event #3 is about two days after of the commencement of the second
321   recovery phase, and the flux tubes had been partially refilled. When the upper
322   ionosphere comes into the sunlight, plasma is supplied through photoionization. So,
323   if the length of time after sunrise is different between the flux tubes at Arase and
324   RBSP, the density may be different. However, as shown in Figure 7d, the MLT is almost
325   same for each L-shells, this effect seems unlikely.

326   Another possibility is the time difference from the end of the main phase. As
327   shown in Figure 7c, the time differences between when the two satellites cross the
328   same L-shells are 0-45 mins. According to the estimate in section 3.1, n_e can increase
329   0-10/cm^3 for such intervals. This effect is too small to interpret the high n_e at the
330   equator. So, we conclude that this difference in density was real, and that there
331   was an increase in density near the equator. Sandhu et al. (2016) statistically
332   analyzed Cluster data and found that the electron density had a localized increase
333   in density near the equator of the plasmatrough. Perhaps even in the partially refilled
334   plasmasphere, the increase in density near the equator may be a common phenomenon.
335   This is an important issue for future research.

336

337   ### 3.4. Application for the Remote Sensing Plasma Mass Density
338   Standing field line resonances (FLRs) in the ULF frequency range are ubiquitous
339   in the magnetosphere, and the frequency of FLRs (f_{FLR}) provides an opportunity to
340   remotely sense the plasma mass density (e.g., Obayashi and Jacobs, 1958; Kitamura
341   and Jacobs, 1968). The procedure for estimating the plasma mass density from the f_{FLR}
342   is to (i) obtain the f_{FLR} from the observation data, (ii) choose a suitable magnetic
343   field model, (iii) select a suitable model for the variation of the plasma mass density
344   along the field line, and (iv) solve the FLR wave equation for the plasma mass density.
345   However, there is very little information about the variation of the density along
346   the field line. Our analysis method makes it possible to obtain this information in
347   the Arase-RBSP era and contributes to the improvement of the accuracy of mass density
348   estimates from the f_{FLR}.

349

350   ## 4. Summary

351   Using plasma waves observed by Arase and RBSP-A and B, we estimated the power-law
352   index m for the field-aligned distributions of n_e for flux tubes at L=3.3-4.1. During
353   and after the 7 Sep 2017 storm event, three conjunction events were studied, in which
354   differences of MLT and UT were respectively <1 hr and <45 mins. In the plume, n_e had
355   comparable values at the higher and the lower latitudes, and the m index was estimated
356   to be ~0. This density profile is expected for diffusive equilibrium. On the other
357   hand, in the inner trough, n_e off the equator was higher than that at near equator,
358   and the m index was estimated as 4-7. Plasma in this region seems to be collisionless.
359   When the satellites were in the plasmatrough with variable n_e, values of n_e off the
360   equator and near the equator were similar; the m index was estimated to be ~0 for
361   both high- and low-density regions. This implies that the plasma transport process
362   might be different between the low-density regions in the variable density structure
363   and the inner trough. In the partially refilled plasmasphere, n_e near the equator was
364   higher than off the equator. This suggests the existence of plasma concentration
365   around the equator.
366

382 **Figure Captions**

383 *Figure 1.*   The positions of Arase (red line) and RBSP-B (blue line) during the interval of 23:30–

384 24:00 UT on 8 Sep 2017 in the L-value- Magnetic Local Time (MLT) plane (top) and L

385 value-Magnetic latitude plane (bottom). The top panel shows exact times of each of the orbits. The

386 small circles and triangles on the orbits respectively indicate positions every five mins of Arase and

387 RBSP-B. Their orbits cross in the afternoon sector. In fact, the difference of MLT and UT comparing

388 at the same L-values are less than 0.5 hr and 15 mins, respectively. Such a conjunction event a gives

389 significant opportunity to compare the electron density between the two different latitudes due to the

390 difference of inclinations of Arase and RBSP.

391

392 *Figure 2*. This figure shows the overall picture of the 7 Sep 2017 storm event and Arase observations

393 shown in this paper. The temporal variations of the Kp and SYM-H indices during the interval from

394 6–10 Sep 2017 are shown in the top and middle panels, respectively. The blue, green, black, and

395 magenta bars in the middle panel indicate the time intervals when the electron densities shown in the

396 bottom panel were observed. The event numbers in parentheses are the event numbers defined in

397 Sections 2-3, 2-4 and 2-5. Arase observations of cold electron density profiles as a function of the

398 McIlwain L-parameter are shown in the bottom panel. The exact times of each observation are

399 provided within the panel. All observations are from outbound orbits. Blue (0): expanded

400 plasmasphere before the storm, extending to L=4.8–5.0. Green (1): the plasmapause pushed further

401 earthward at L=2.5 immediately after the second main phase. Black (2): the severely eroded

402 plasmasphere with the plasmapause being pushed even further at L=1.6–1.7. Magenta (3): partial

403 recovery of the severely eroded plasmasphere at 1.5 days after density profile #2 (black).

404

405 *Figure 3.*   Spectrograms of radio and plasma waves obtained by Arase (a) and RBSP-B (b) from

406 23:20 UT on 8 Sep to 00:10 UT on 9 Sep 2017. In both panels, narrow-banded UHR waves are

407 clearly found and indicated by the white lines and arrows. In 3a, the UHR frequency was decreasing

408 gradually from 300 to 100 kHz during 23:20–23:48 UT because Arase was in an outbound pass, and

409 then suddenly jumped up to ~150 kHz at 23:49 UT. This implies that the satellite passed the

410 boundary between low- and high-density regions, which correspond to the inner trough and plasma

411 plume, respectively. In 3b, The observation time is divided into a period showing the high UHR

412 frequency before 23:52 UT and a period showing a low UHR frequency after 23:52 UT. Each

413 corresponds to the times the satellite flying into the high-density plume and the low-density inner

414 trough. The lower three panels show L-value (c), magnetic local time (MLT) (d), and magnetic

415 latitudes (e) of Arase and RBSP-B. They are calculated using the Olson-Pfitzer-Quitet (OPQ 77)

416 magnetic field model (Olson and Pfitzer, 1977). The thick portion of the lines indicate the position of

417 the satellite orbits when their L-values are in the range of L=3.3–4.1. The time is 23:46–23:59 UT

418   for Arase and 23:31–24:00 UT for RBSP-B.

419

420   *Figure 4.*   (top) L-value profile of the electron density inferred from f_{UHR} using the plasma wave

421   observations during 23:30–24:00 UT on 8 Sep 2017. The red and blue dots indicate Arase and

422   RBSP-B observations, respectively. (bottom) L-value profile of the power-law index *m* (defined in

423   Section 2.3) which is estimated using differences of electron density and magnetic latitude between

424   Arase and RBSP-B.

425

426   *Figure 5.*   Spectrograms of radio and plasma waves obtained by Arase (a) and RBSP-B (b),

427   L-value (c), magnetic local time (MLT) (d) and magnetic latitude (e) of Arase and

428   RBSP-B during 14:15-15:05 UT on 8 Sep 2017. The locations of the satellites are

429   computed by using the Tsyganenko 2004 storm model. The format of this figure is same

430   as that of Figure 3. The UHR frequency fluctuates with a time scale in the range from

431   1 to 10 mins. This observation is during the second main phase, with the plasmapause

432   seen at L=2.5, thus, the fluctuations of f_{UHR} imply existence of small-scale structures

433   in the plasmatrough.

434

435   *Figure 6.*   (top) L-value profiles of the electron density inferred from f_{UHR} using the plasma wave

436   observations during 14:15–15:05 UT on 8 Sep 2017. The red and blue dots indicate Arase and

437   RBSP-B, respectively. (bottom) L-value profile of the power-law index *m* which is estimated using

438   differences of electron density and magnetic latitude between Arase and RBSP-B. Between L=3.3

439   and 3.9, the changes in electron density observed by two satellites seems to be correlated, thus the *m*

440   index ~0 in both the high- and low-density regions.

441

442   *Figure 7.*   Spectrograms of radio and plasma waves obtained by Arase (a) and RBSP-B (b), L-value

443   (c), magnetic local time (MLT) (d), and magnetic latitude (e) of Arase and RBSP-B during 13:40–

444   14:30 UT on 10 Sep 2017. The locations of the satellites are computed using OPQ 77 model. The

445   format of this figure is same as that of Figure 3. The f_{UHR} observed by Arase (RBSP-A) gradually

446   decreased (increased). This corresponds to the gradual electron density gradient with distance in the

447   plasmasphere.

448

449   *Figure 8.*   L-value profiles of the electron density and the power-law index *m* during 13:40–14:30

450   UT on 10 Sep 2017. The format of this figure is same as that of Figure 4. Due to the limits of the

451   frequency resolution of the spectrogram shown by Figure 7b, the RBSP-B observations are aligned

452   in a stepped shape. The time of this event is about two days after the commencement of the second

453   recovery phase of the storm, thus the observations depict the density profiles of a partially refilled

454   plasmasphere. The negative values of *m* index indicate higher electron density at near the equator

455   than that off the equator.

456

457

458   **References**

459   Angerami, J. J., and D. L. Carpenter (1966), Whistler studies of the plasmapause in

460   the magnetosphere: 2. Electron density and total tube electron content near the knee

461   in the magnetospheric ionization, J. Geophys. Res., 71, 711-725.

462

463   Denton, R. E., J. Goldstein, J. D. Menietti, and S. L. Young (2002), Magnetospheric

464   electron density model inferred from Polar plasma wave data, J. Geophys. Res., 107,

465   1386, doi:10.1029/2001JA009136.

466

467   Denton, R. E., et al. (2009), Field line distribution of density at L = 4.8 inferred

468   from observations by CLUSTER, Ann. Geophys., 27, 705-724,

469   doi:10.5194/angeo-27-705-2009.

470

471   Eviatar, A., Lenchek, A. M., & Singer, S. F. (1964). Distribution of Density in an

472   Ion-Exosphere of a Nonrotating Planet. The Physics of Fluids, 7(11), 1775-1779.

473   https://doi.org/10.1063/1.2746776.

474

475   Goldstein, J., R. E. Denton, M. K. Hudson, E. G. Miftakhova, S. L. Young, J. D. Menietti,

476   and D. L. Gallagher (2001), Latitudinal density dependence of magnetic field lines

477   inferred from Polar plasma wave data, J. Geophys. Res., 106, 6195-6202,

478   doi:10.1029/2000JA000068.

479

480   Goldstein, J., B. R. Sandel, W. T. Forrester, and P. H. Reiff, IMF-driven plasmasphere

481   erosion of 10 July 2000, Geophys. Res. Lett., 30(3), 1146, doi:10.1029/2002GL016478,

482   2003.

483

484   Huang, X., B. Reinisch, P. Song, J. L. Green, D. L. Gallagher (2004), Developing an

485   empirical density model of the plasmasphere using IMAGE/RPI observations, Advances

486   in Space Research, 33(6):829-832, DOI: 10.1016/j.asr.2003.07.007.

487

488   Kasahara, Y., Kasaba, Y., Kojima, H., Yagitani, S., Ishisaka, K., Kumamoto, A., et

489   al. (2018). The Plasma Wave Experiment (PWE) onboard the Arase (ERG) satellite. Earth,

490   Planets and Space, 70(1), 86. https://doi.org/10.1186/s40623‑018‑0842‑4

491

492   Kletzing, C. A., Kurth, W. S., Acuna, M., MacDowall, R. J., Torbert, R. B., Averkamp,
493   T., et al. (2013). The Electric and Magnetic Field InstrumentSuite and Integrated
494   Science (EMFISIS) on RBSP. Space Science Reviews, 179(1‑4), 127-181.
495   https://doi.org/10.1007/s11214013‑9993‑6

496

497   Kumamoto, A., Tsuchiya, F., Kasahara, Y., Kasaba, Y., Kojima, H., Yagitani, S., et
498   al. (2018). High Frequency Analyzer (HFA) of Plasma Wave Experiment (PWE) onboard
499   the Arase spacecraft. Earth, Planets and Space, 70(82).
500   https://doi.org/10.1186/s40623‑018‑0854‑0

501

502   Matsuoka A, Teramoto M, Nomura R, Nose M, Fujimoto A, Tanaka Y, Shinohara M, Nagatsuma
503   T, Shiokawa K, Obana Y, Miyoshi Y, Mita M, Takashima T, Shinohara I (2018) The Arase
504   (ERG) magnetic field investigation. Earth Planets Space 70:43.
505   https://doi.org/10.1186/s40623–018–0800–1

506

507   Mauk, B. H., Fox, N. J., Kanekal, S. G., Kessel, R. L., Sibeck, D. G., & Ukhorskiy,
508   A. (2013). Science objectives and rationale for the Radiation Belt Storm Probes
509   Mission. Space Science Reviews, 179(1–4), 3-27.
510   https://doi.org/10.1007/s11214–012–9908–y.

511

512   McIlwain, C. E. (1961). Coordinates for mapping the distribution of magnetically
513   trapped particles. Journal of Geophysical Research, 66(11), 3681-3691.
514   https://doi.org/10.1029/JZ066i011p03681

515

516   Miyoshi Y, Ono T, Takashima T, Asamura K, Hirahara M, Kasaba Y, Matsuoka A, Kojima
517   H, Shiokawa K, Seki K, Fujimoto M, Nagatsuma T, Cheng CZ, Kazama Y, Kasahara S, Mitani
518   T, Matsumoto H, Higashio N, Kumamoto A, Yagitani S, Kasahara Y, Ishisaka K, Blomberg
519   L, Fujimoto A, Katoh Y, Ebihara Y, Omura Y, Nose Hori T, Miyashita Y, Tanaka Y–M,
520   Segawa, ERG working group (2012) The energization and radiation in geospace (ERG)
521   project. In: Summers D, Mann IR, Baker DN, Schulz M (eds) Dynamics of the Earth's
522   radiation belts and inner magnetosphere. American Geophysical Union, Washington.
523   https://doi.org/10.1029/2012gm001304

524

525   Miyoshi Y, Kataoka R, Ebihara Y (2016) Flux enhancement of relativistic electrons

526 associated with substorms. In: Balasis G, Daglis IA, Mann IR (eds) Waves, particles,
527 and storms in geospace. Oxford Press, Oxford, pp 333-353

528

529 Miyoshi, Y., Shinohara, I., Takashima, T., Asamura, K., Higashio, N., Mitani, T.,
530 et al. (2018a). Geospace Exploration Project ERG. Earth, Planets and Space, 70(1),
531 101. https://doi.org/10.1186/s40623-018-0862-0

532

533 Miyoshi, Y., Hori, T., Shoji, M., Teramoto, M., Chang, T. F., Segawa, T., et al. (2018b).
534 The ERG Science Center. Earth, Planets and Space, 70(1), 96.
535 https://doi.org/10.1186/s40623-018-0867-8

536

537 Obana, Y., F. W. Menk, and I. Yoshikawa (2010), Plasma refilling rates for L = 2.3-
538 3.8 flux tubes, J. Geophys. Res., 115, A03204, doi:10.1029/2009JA014191.

539

540 Obana, Y., Maruyama, N., Shinbori, A., Hashimoto, K. K., Fedrizzi, M., Nosé, M., et
541 al. (2019). Response of the ionosphere-plasmasphere coupling to the September
542 2017storm: What erodes the plasmasphere so severely?, Space Weather, 17.
543 https://doi.org/10.1029/ 2019SW002168

544

545 Olson, W. P., and K. A. Pfitzer, Magnetospheric magnetic field modeling, Annual
546 Scientific Report, AFOSR Contract No. F44620-75-C-0033, 1977.

547

548 Reinisch, B. W., X. Huang, P. Song, G. S. Sales, S. F. Fung, J. L. Green, D. L. Gallagher,
549 and V. M. Vasyliunas (2001), Plasma Density Distribution Along the Magnetospheric
550 Field: RPI Observations From IMAGE, Geophys. Res. Lett., 28, 24, 4521-4524,
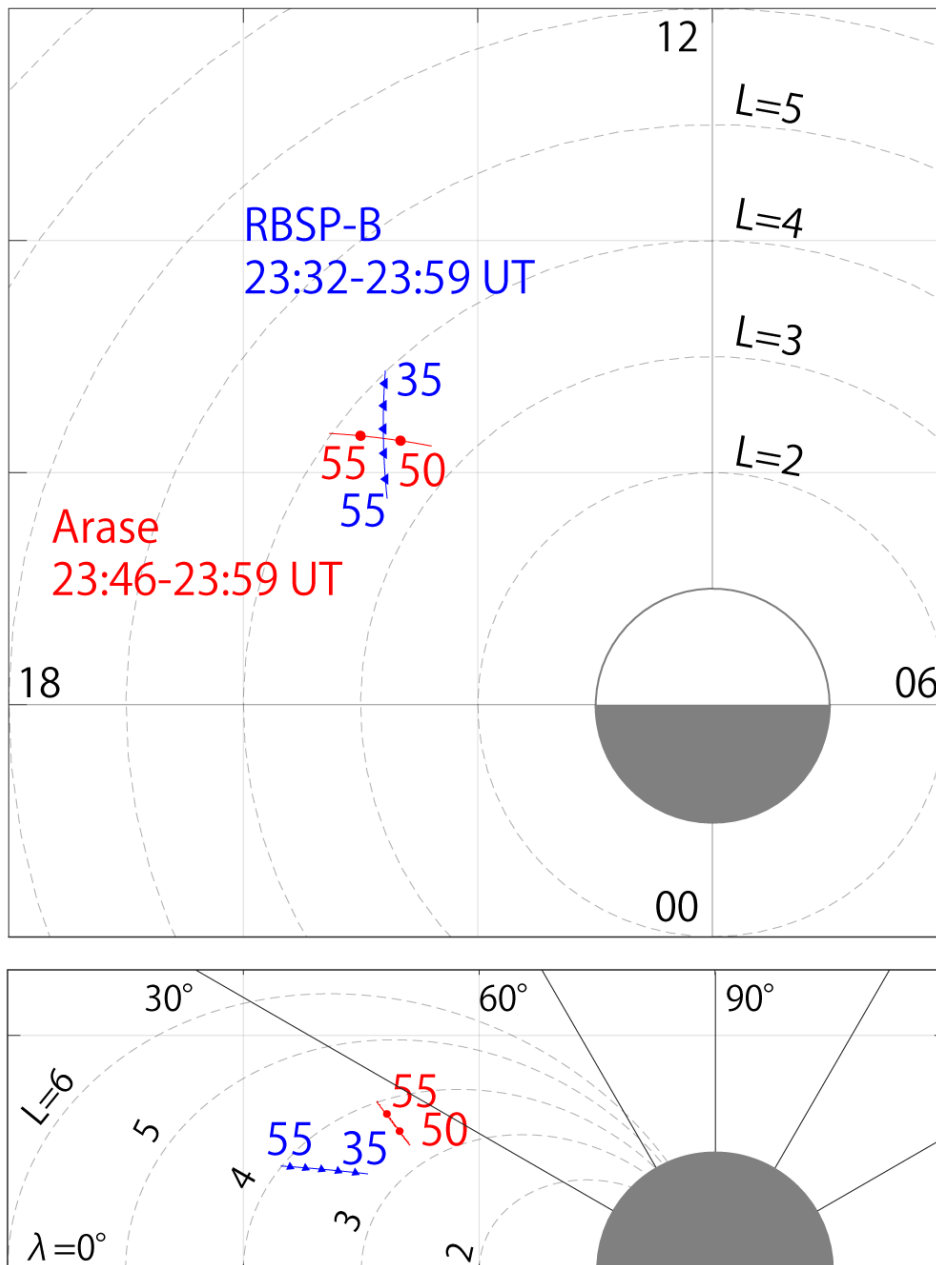551 doi:10.1029/2001GL013684.

552

553 Sandhu, J. K., T. K. Yeoman, R. C. Fear, and I. Dandouras (2016), A statistical study
554 of magnetospheric electron density using the Cluster spacecraft, J. Geophys. Res.
555 Space Physics, 121, 11,042-11,062, doi:10.1002/2016JA023397.

556

557 Song, P., B. W. Reinisch, X. Huang, J. L. Green (2005), 'Magnetospheric Active Wave
558 Measurements', COSPAR Colloquia Series, Volume 16, Frontiers in Magnetospheric Plasma
559 Physics: Celebrating 10 Years of Geotail Operation, pp. 235-246,
560 doi.org/10.1016/S0964-2749(05)80036-8.

561

562   Takahashi, K., R. E. Denton, R. R. Anderson, and W. J. Hughes (2004), Frequencies
563   of standing Alfve´n wave harmonics and their implication for plasma mass distribution
564   along geomagnetic field lines: Statistical analysis of CRRES data, J. Geophys. Res.,
565   109, A08202, doi:10.1029/2003JA010345.
566
567   Tsyganenko, N. A. and Sitnov, M. I.: Modelling the dynamics of the inner magnetosphere
568   during strong geomagnetic storms, J. Geophys. Res., 110, A03208,
569   doi:10.1029/2004JA010798, 2005.
570

Arase and RBSP-B Orbits   8 Sep 2017

572   Figure 1
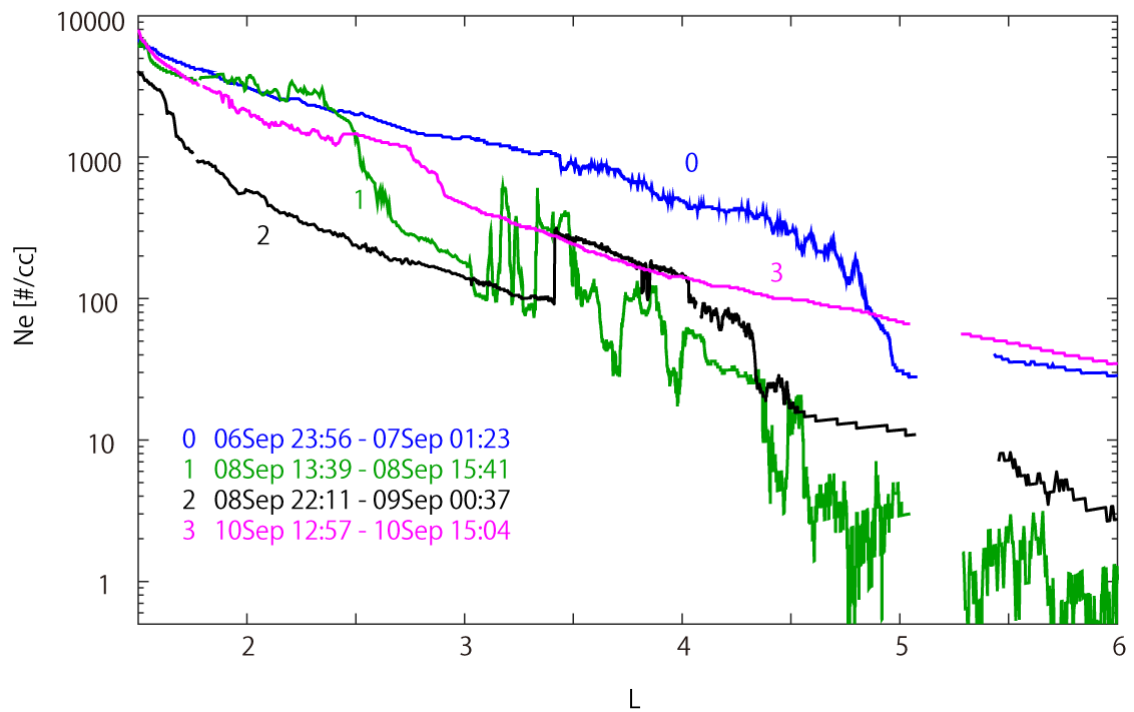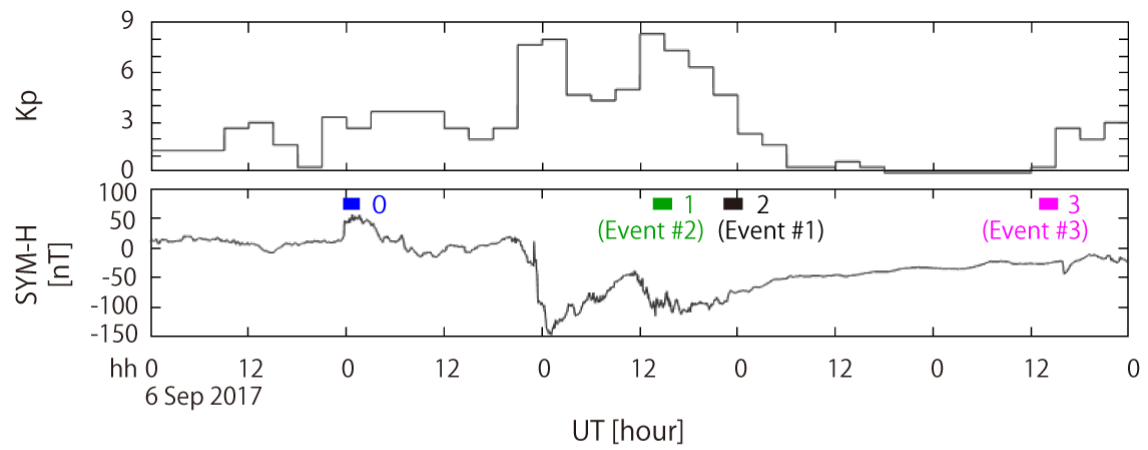
574

575

576

577

578

579 Figure 2

580

ARASE - RBSP B   2017-09-08   23:20

(a) Arase PWE/HFA [kHz]

(b) RBSP-B/EMFISIS [kHz]

(c) L-value OPQ77

(d) MLT [hour]

(e) Mlat [deg]

581

582

583   Figure 3

ARASE-RBSP B   2017-09-08   23:20UT

ARASE : Red
RBSP B : Blue

584

585

586   Figure 4

587

ARASE- RBSP B   2017-09-08   14:15

(a) Arase PWE/HFA [kHz]

(b) RBSP-B/EMFISIS [kHz]

(c) L-value T 04s

(d) MLT [hour]

(e) Mlat [deg]

RBSP-B

Arase

hh:mm
08 Sep

588

589

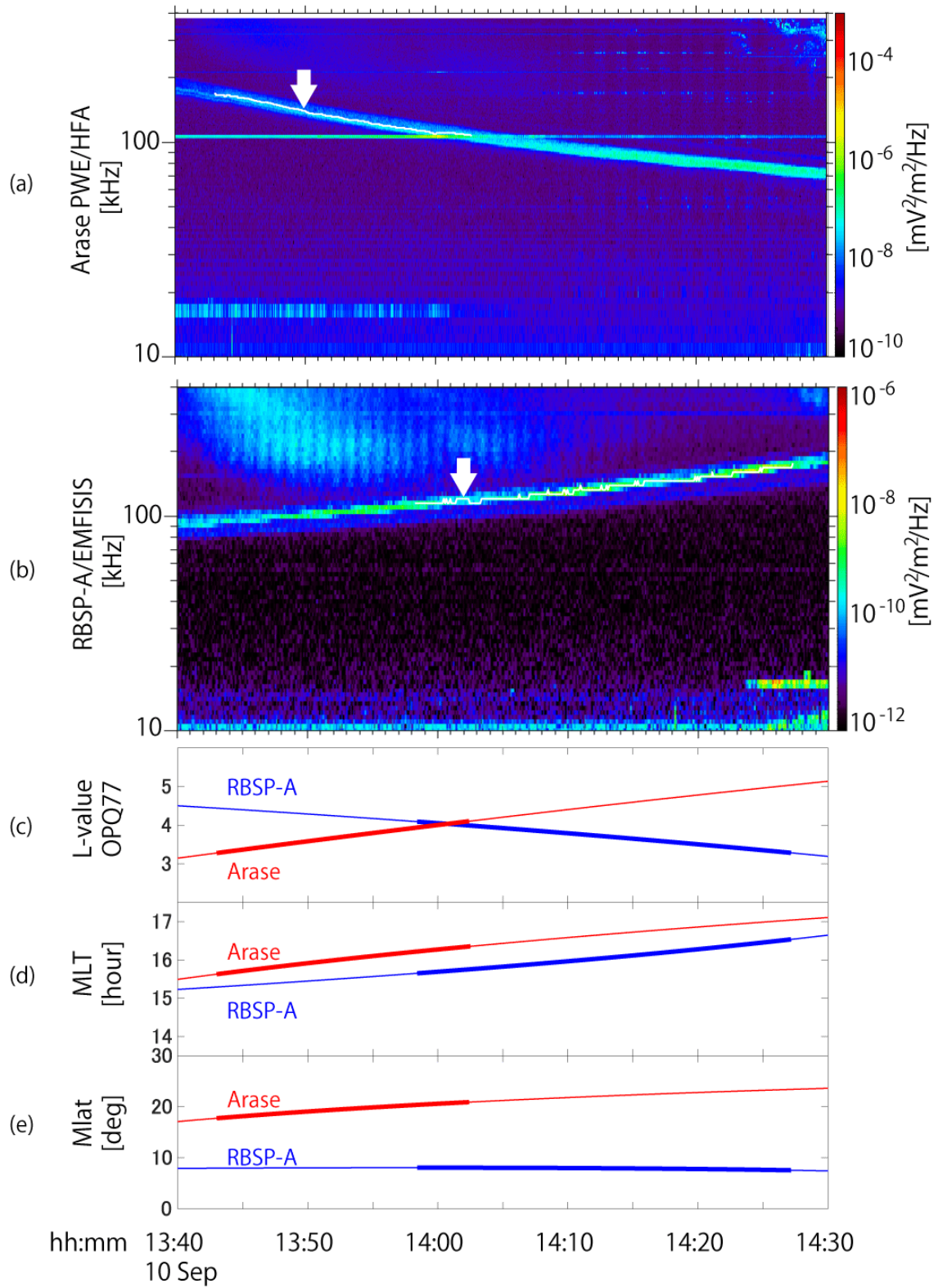590   Figure 5

591
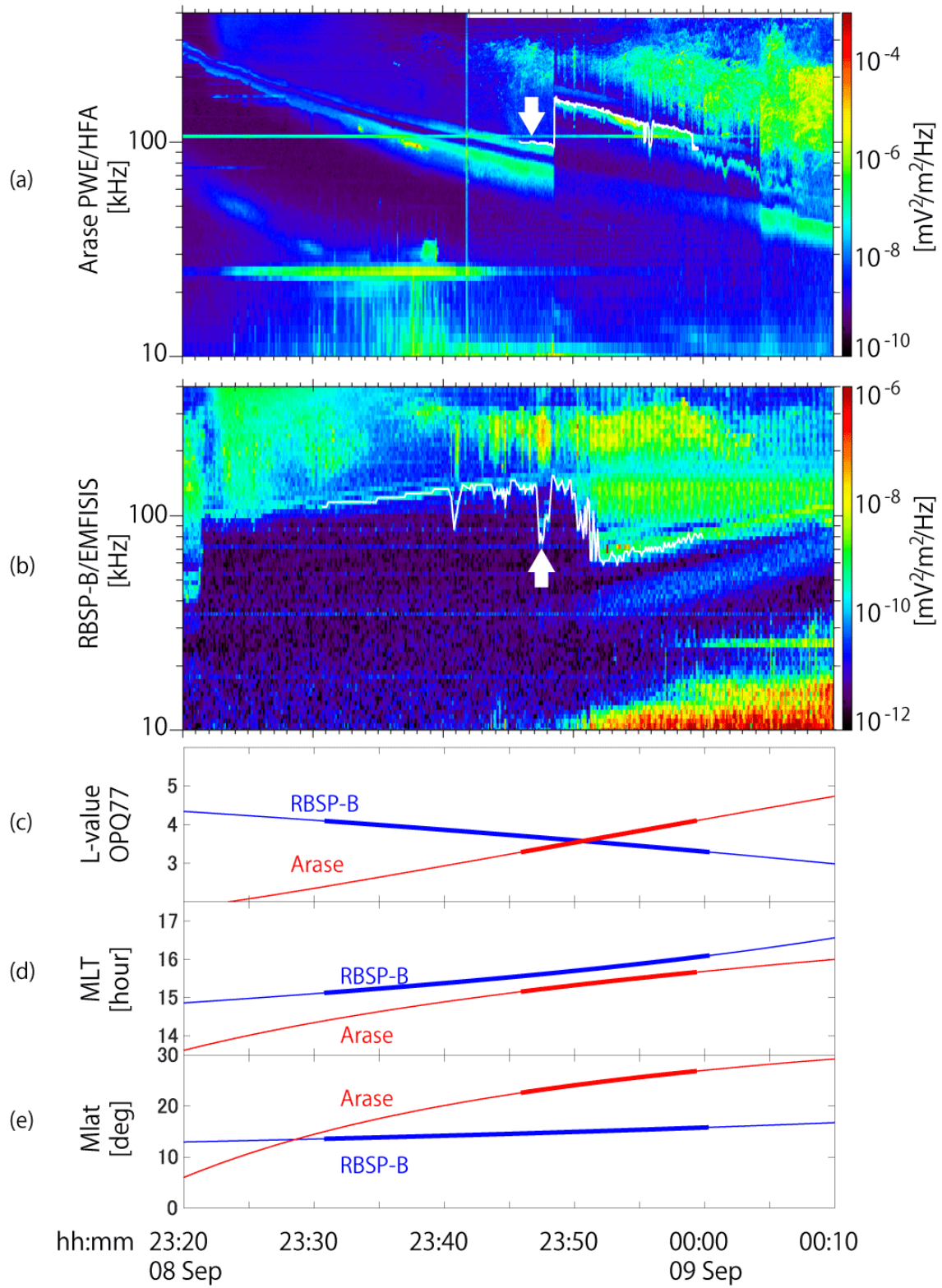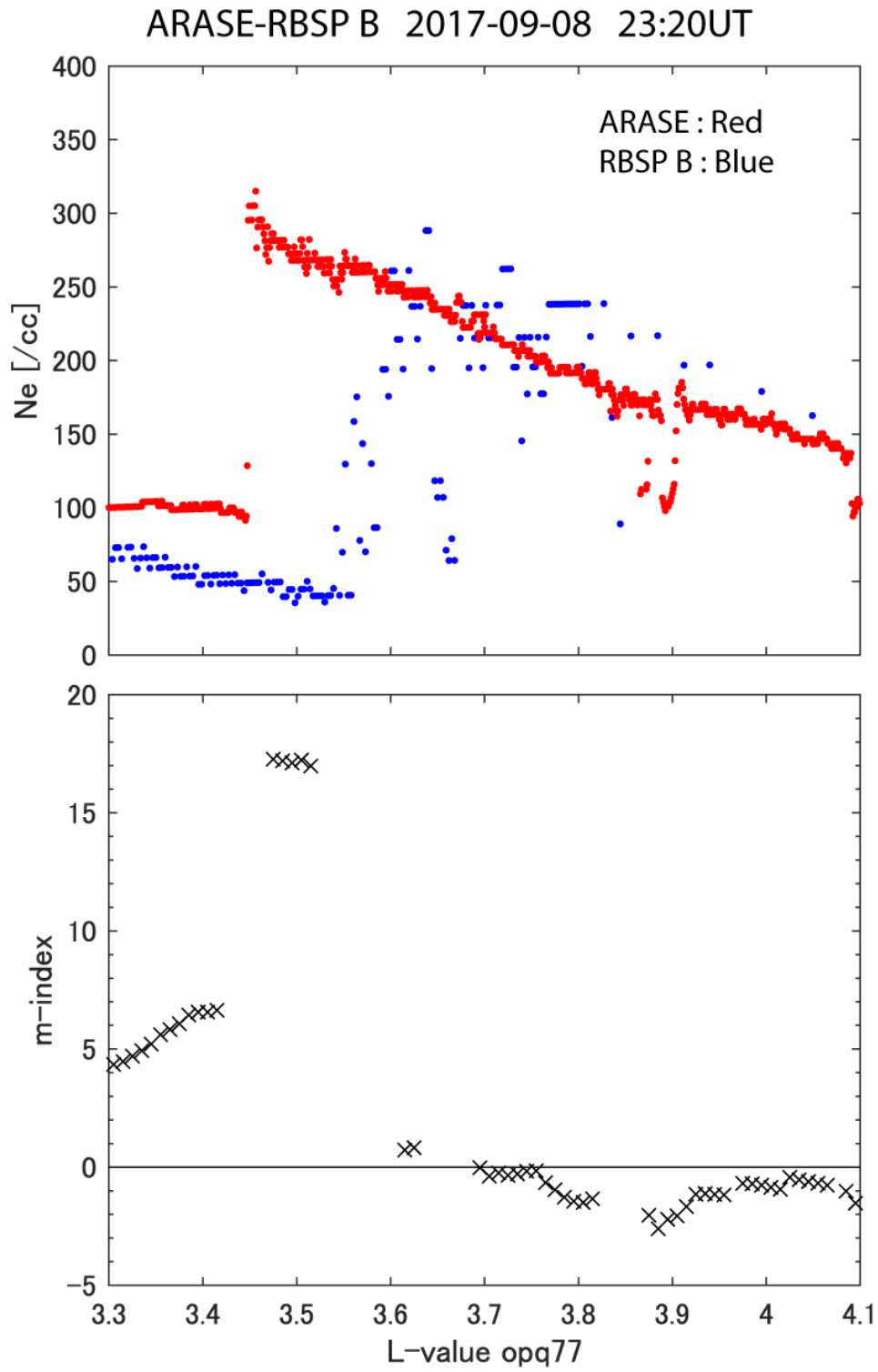
ARASE-RBSP B   2017-09-08   14:15UT
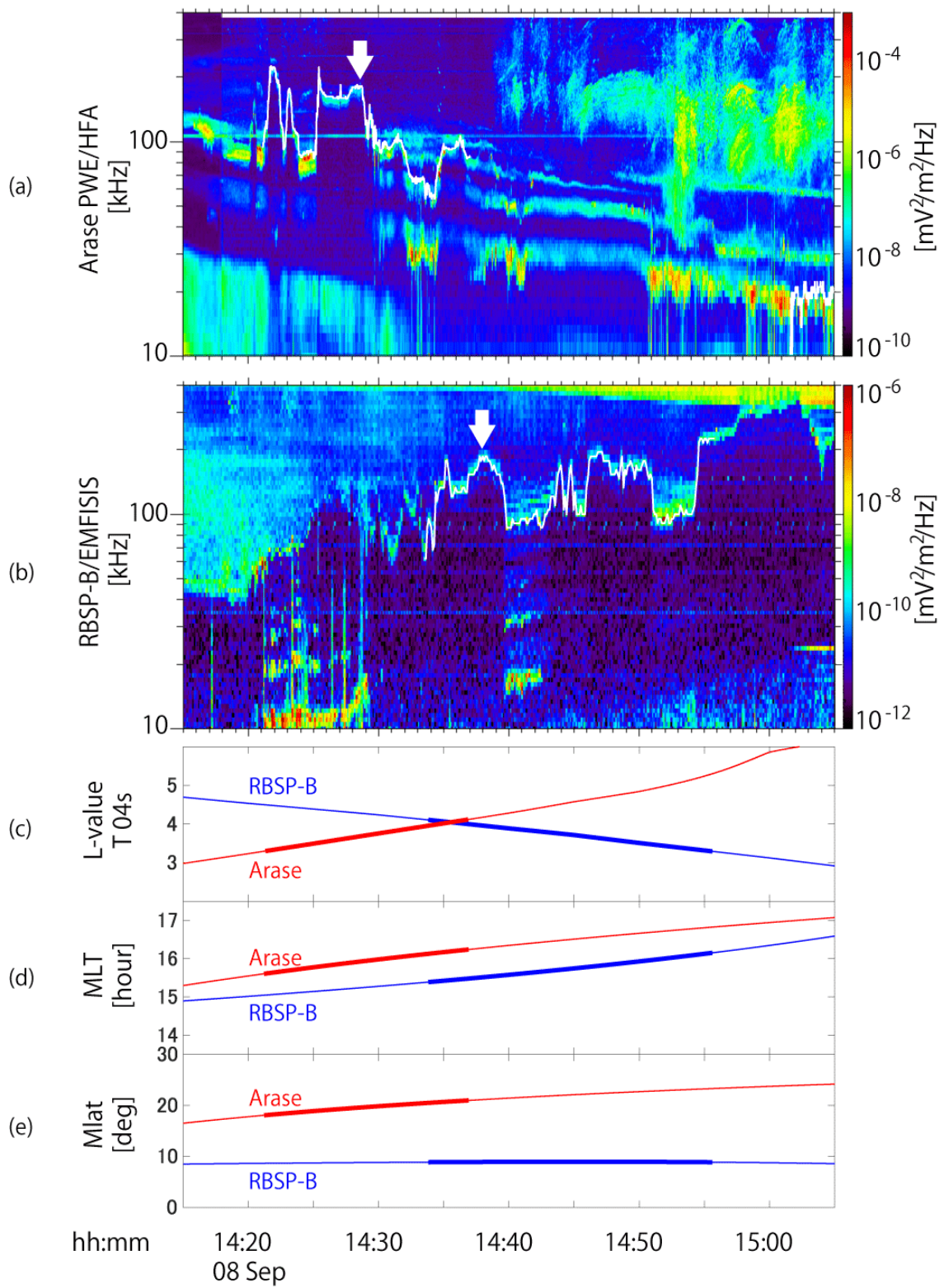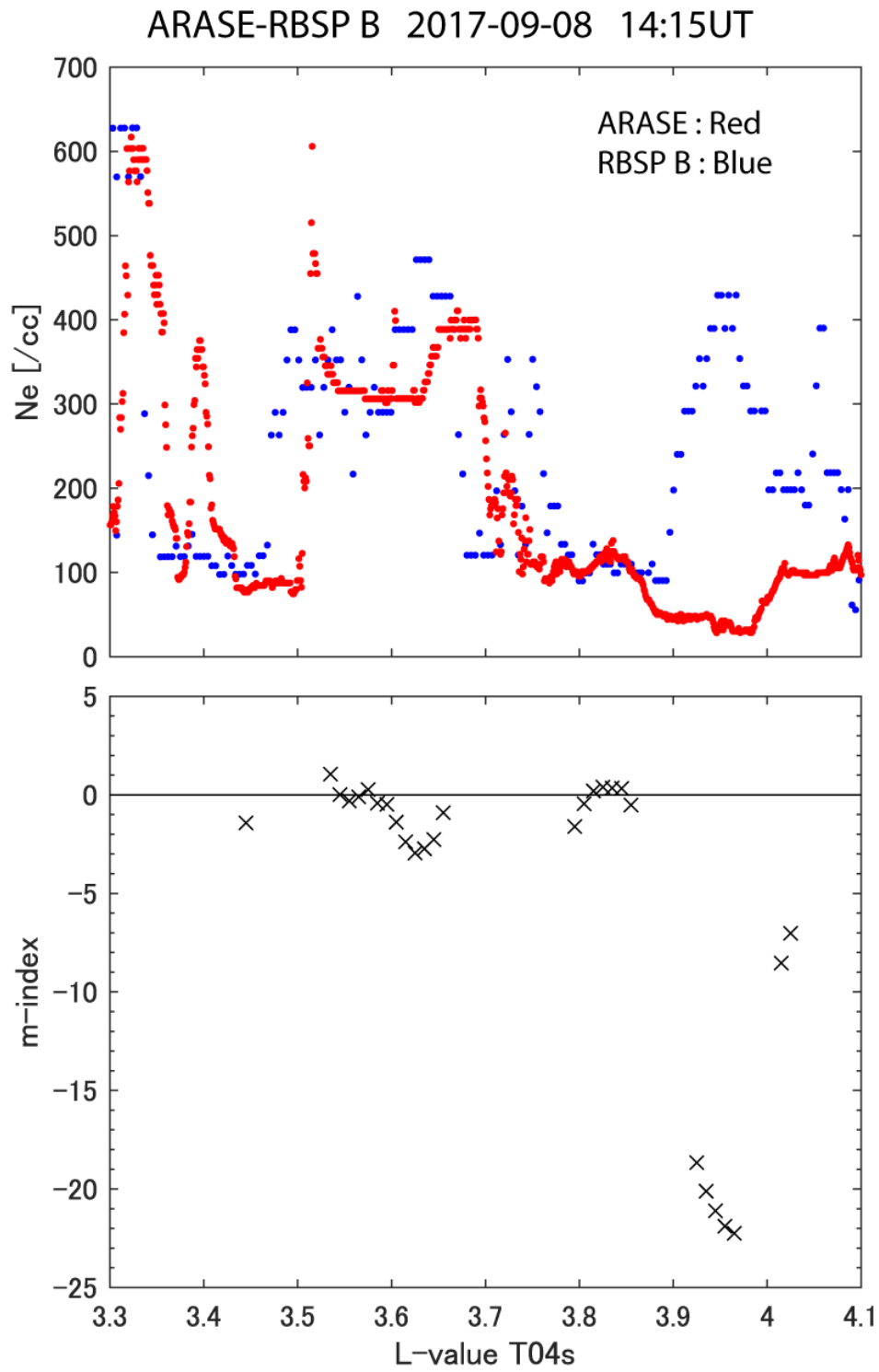
592
593

594   Figure 6

595

ARASE - RBSP A 2017-09-10 13:40

596

597   Figure 7

ARASE-RBSP A   2017-09-10   13:40UT

598

599

600   Figure 8